DE GRUYTER Nanophotonics 2017; 6(1): 289–297

Research article Open Access

Claudia Gritti[a], Søren Raza[a], Shima Kadkhodazadeh, Beata Kardynal, Radu Malureanu, N. Asger Mortensen and Andrei V. Lavrinenko*

Broadband infrared absorption enhancement by electroless-deposited silver nanoparticles

DOI 10.1515/nanoph-2016-0114
Received April 5, 2016; revised May 12, 2016; accepted May 24, 2016

Abstract: Decorating semiconductor surfaces with plasmonic nanoparticles (NPs) is considered a viable solution for enhancing the absorptive properties of photovoltaic and photodetecting devices. We propose to deposit silver NPs on top of a semiconductor wafer by a cheap and fast electroless plating technique. Optical characterization confirms that the random array of electroless-deposited NPs improves absorption by up to 20% in a broadband of near-infrared frequencies from the bandgap edge to 2000 nm. Due to the small filling fraction of particles, the reflection in the visible range is practically unchanged, which points to the possible applications of such deposition method for harvesting photons in nanophotonics and photovoltaics. The broadband absorption is a consequence of the resonant behavior of particles with different shapes and sizes, which strongly localize the incident light at the interface of a high-index semiconductor substrate. Our hypothesis is substantiated by examining the plasmonic response of the electroless-deposited NPs using both electron energy loss spectroscopy and numerical calculations.

Keywords: plasmonic nanoparticles; absorption enhancement; random nanoparticles; electroless plating; electron energy loss spectroscopy.

1 Introduction

In the last 20 years, there has been an increasing interest in plasmonics, with an attention on applications and new emerging directions [1, 2]. The fields of application include molecular sensing [3–5] and tagging [6, 7], focusing of light [8, 9], near-field optical microscopy [10, 11], subwavelength photonics [12, 13], structural colors [14, 15], and optical metamaterials [16, 17]. In particular, the use of plasmons for hot-electron science and photovoltaics is strongly appealing [18–23]. Plasmonics is now considered a significant approach to enhancing the light-trapping properties of thin-film solar cells. Metal nanoparticles (NPs) support surface plasmon modes, which are used to efficiently couple light into the optical modes of the underlying or surrounding semiconductor. The excitation of localized surface plasmons (LSPs) gives rise to pronounced optical absorption, field localization, and anomalous scattering phenomena [24–27]. The resonance wavelength depends on the size, shape, and local dielectric environment of the NP. Thus, absorption enhancement in a defined wavelength range can be achieved using such knobs to tune the LSP resonance [3]. It is well known that for spherical-like gold and silver NPs the resonances typically fall into the visible-light spectrum region [18, 19, 28]. However, it is also worth emphasizing that an LSP resonance red-shift can be achieved by increasing the particle aspect ratio [29] and the size of the NPs [30] or by employing particle ensembles and the hybridization of particles [31–33]. In this work, we are interested in light absorption in the near-infrared (IR) region of the solar spectrum to harvest photons that would otherwise be wasted because of the intrinsic limit (bandgap) of semiconductor materials.

[a]**Claudia Gritti and Søren Raza:** These authors contributed equally to this work.
***Corresponding author: Andrei V. Lavrinenko,** Department of Photonics Engineering, Technical University of Denmark, 2800 Kgs. Lyngby, Denmark, e-mail: alav@fotonik.dtu.dk
Claudia Gritti and Radu Malureanu: Department of Photonics Engineering, Technical University of Denmark, 2800 Kgs. Lyngby, Denmark
Søren Raza: Centre for Nano Optics, University of Southern Denmark, Campusvej 55, 5230 Odense M, Denmark
Shima Kadkhodazadeh: Center for Electron Nanoscopy (CEN), Technical University of Denmark, 2800 Kgs. Lyngby, Denmark
Beata Kardynal: Peter Grünberg Institute (PGI-9), Research Centre Jülich, JARA FIT, 52425 Jülich, Germany
N. Asger Mortensen: Department of Photonics Engineering, Technical University of Denmark, 2800 Kgs. Lyngby, Denmark; and Center for Nanostructured Graphene (CNG), Technical University of Denmark, 2800 Kgs. Lyngby, Denmark

Metallic NPs can be placed in the vicinity of the active layer of a thin-film solar cell, by means of the transparent electrode-semiconductor interface, and used as active nanoantennas absorbing photons with energy below the semiconductor bandgap ($\hbar\omega<E_g$) but above the metal work function W_b ($\hbar\omega>W_b$) [34–37] (see the simplified mechanism of plasmonic particle photocurrent generation sketched in Figure 1A). Once the photon is absorbed by the metallic NP, an electron close to the Fermi level can be excited to the conduction band (E_c) of the semiconductor. This is referred to as a sub-bandgap absorption process: the involved photon energy $\hbar\omega$ is smaller than the usual transition from the valence band (E_v) to the conduction band (i.e. $\hbar\omega<E_g=E_c-E_v$). Photon absorption in such a case may result in the photoemission of an electron from the metal NP into the semiconductor. This mechanism allows the harvesting of photons with a sub-bandgap energy usually not exploited by a typical photovoltaic device (Figure 1A).

The possibility of photoemission through the near-IR plasmonic excitation has been discussed and experimentally demonstrated [34, 37–46], proving the existence of different ways to extend the spectral response of a photovoltaic device. However, in most cases, the costly and CMOS-incompatible electron-beam lithography is used. Although key to the realization and exploration of plasmon phenomena, electron-beam lithography clearly jeopardizes the application potential of plasmon nanostructures. In this article, we report an alternative approach of mass fabrication of silver NPs on top of the semiconductor interface, which is known as the electroless deposition of metal. Electroless plating has attracted great interest due to the simplicity of operation, cost-effectiveness, high throughput, and the limited requirements of elaborate equipment [47, 48]. Over the last few years, in contrast to complex and expensive vacuum methods of metallization, electroless deposition, as an alternative to colloidal solutions and self-assembly techniques, has also been used as a worthwhile method for the fabrication of metallic NPs on different surfaces [49–52].

The structure of the article is as follows. In Section 2, we describe the electroless deposition of silver NPs on a GaAs wafer. In Section 3, we report the results of sample characterization. We observe the pronounced and spectrally very flat enhancement of absorption in a broad range of wavelengths from 900 nm (just above the GaAs bandgap) up to 2 µm. In Section 4, we provide the theoretical interpretation of our experimental results. The topology information and electromagnetic near-field properties of the deposited NPs are obtained using electron energy loss spectroscopy (EELS) as presented in Section 5. Finally, conclusions are given in Section 6.

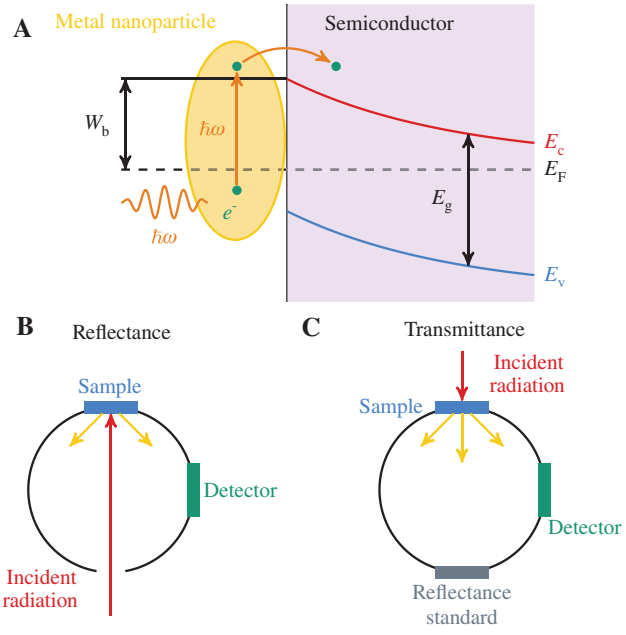

Figure 1: Illustration of the NP electron emission mechanism (A) and illustration of the working principle of the integrating sphere for reflectance (B) and transmittance (C) measurements, respectively.

2 Electroless plating

Arrays of silver NPs are deposited on the surface of an n-doped GaAs wafer. The silver plating solution is composed of silver nitrate ($AgNO_3$) diluted in water at 2% and hydrofluoric acid (HF) at 5% concentration. The density of silver coating can vary with the time of deposition and solution concentrations. More precise descriptions of recipes have been reported elsewhere along with the studies of morphology of the silver coating as well as individual particle deposition [51, 52].

The deposition leads to random arrays of particles, as shown in the scanning electron microscopy (SEM) images of Figure 2. The randomness guarantees the homogeneity of the particle distribution. However, the unknown parameters so far are the density of silver NPs and their sizes. The former has an optimal value: the density needs to be sufficiently large to provide a valuable yield in absorption enhancement yet well below the percolation threshold so that the film of the particles remains transparent to the light illuminating the underlying semiconductor surface. The average size of the particles is also a very sensitive parameter, as it needs to provide a reasonable absorption

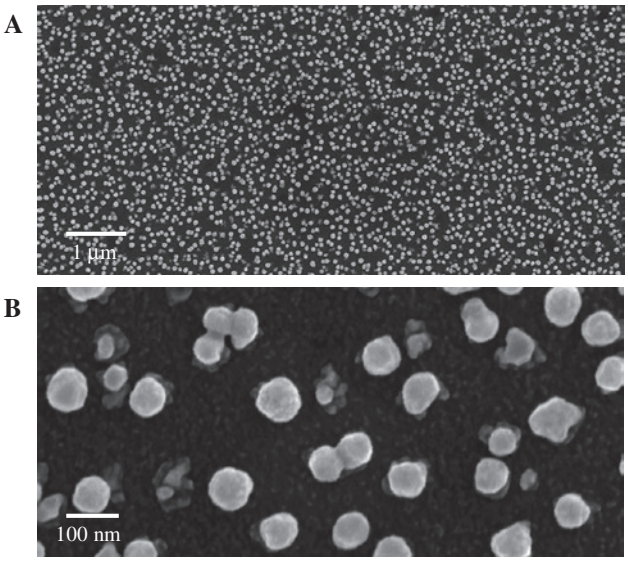

Figure 2: SEM images of silver NPs deposited by electroless plating on GaAs substrate. (A) Overview and (B) zoom-in images. Top view of typical NP shapes such as circular, elliptical, and overlapping dimers.

cross-section while adequately red-shifting the LSP resonances into the near-IR range [53]. The LSP resonances of the NPs experience a red shift due to the surrounding media, which in our case constitutes an optically thick GaAs substrate and a 100-nm-thick transparent indium-tin oxide (ITO) contact layer.

An example of a fabricated sample is shown in Figure 2. The deposited NPs have an average size of 70 nm and cover 21% of the surface's area. The typical cross-section shapes of the NPs range from circular to elliptical while also featuring particle dimers and trimers with tiny gaps.

3 Optical characterization

Our main emphasis is the change in the IR absorbance due to the presence of the particles. To determine the absorption spectra, we use a 2-inch integrating sphere. The instrument consists of a hollow spherical cavity with its interior covered by a diffuse white-reflective coating. Therefore, all photons entering the sphere are diffusively scattered and collected by an optical fiber connected to a spectrometer (near-IR range). Such geometry of the measurement ensures a fair sampling of the light that has not been absorbed in the sample [i.e. all specularly and diffusively scattered light either transmitted (T) or reflected (R) by the sample]. Due to the flux conservation, the absorbance (A) is calculated as $A=1-R-T$. During the measurements, the sample is always placed outside the sphere while attached to the entrance port; the characterization configurations are sketched in Figure 1B and C.

In terms of potential photovoltaic applications, the most interesting photon-energy range is limited by the height of the Schottky barrier between the particle (Ag) and the semiconductor (n-GaAs). It is 0.63 eV [54] or 1968 nm in terms of the wavelength. We also monitor the visible range to ensure that no pronounced reductions in absorption happen due to the presence of the particles.

We measure the reflectance and transmittance from the sample shown in Figure 2 along with a reference sample comprising an identical n-GaAs substrate but without NPs. Before the measurements, both samples are coated with a 100-nm-thick layer of ITO. The measured transmittance and reflectance spectra along with the calculated absorbance spectrum are shown in Figure 3A–C, respectively.

In the wavelength region 900–2000 nm (beyond the bandgap of n-GaAs), the reflectance is increased by up

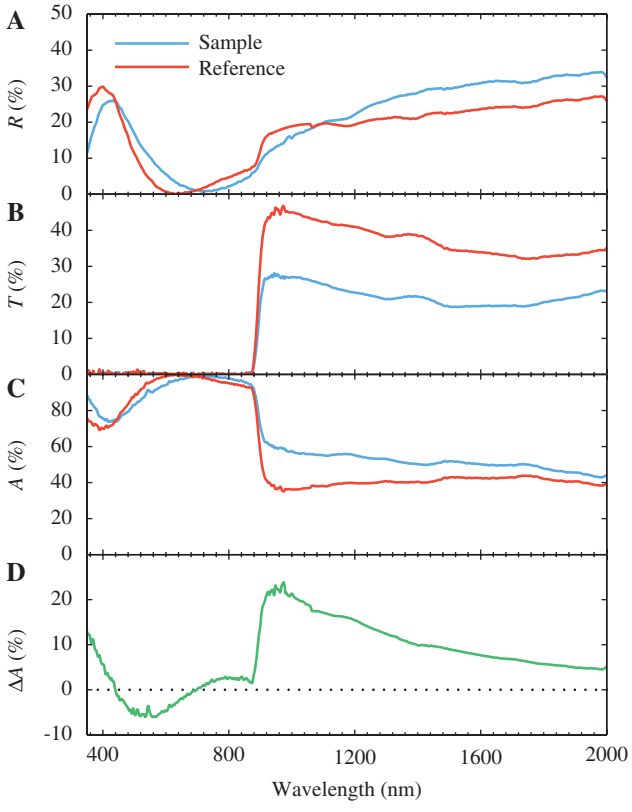

Figure 3: Spectral characterization of samples. (A) Reflectance R, (B) transmittance T, and (C) absorbance A spectra of ITO semiconductor sample with silver NPs (blue) and reference sample without NPs (red). (D) Difference in absorbance ΔA between the sample and the reference.

to 5%–7% (Figure 3A), whereas the transmittance drops by more than 20% (Figure 3B). The presence of silver NPs results in a large (up to 25%) and very broad absorbance enhancement (Figure 3C), spanning the entire IR range and also some parts of the visible spectral range. We also note that no pronounced changes in the reflectance in the visible range are observed, suggesting that the screening effect of the NPs will not affect adversely the operation of devices for potential photovoltaic applications.

Plotting the difference in absorbance between the samples with and without NPs (Figure 3D) further visualizes the plasmonic enhancement. We observe no resonant features, but rather we find a wide and flat plateau in the spectrum. We speculate that such spectral behavior of the absorption enhancement results from the different contributions of a random distribution of NPs, which features NPs of various sizes and shapes along with various particle-dimer configurations. To further investigate the effect, the main elements characterizing the NP distribution of the sample under study (single, elongated, and overlapping dimers) are modeled numerically with the aid of classical electrodynamics and furthermore examined experimentally using EELS.

4 Simulations

To interpret the observed spectra, we complement the experimental results with theoretical simulations using a commercially available finite-element software (COMSOL), which solves the classical Maxwell equations. We are interested in understanding the basic mechanism behind the observed broadband absorbance enhancement in the near-IR spectral range. To this end, we focus our simulations on the most characteristic NP shapes of the sample (i.e. circular and elliptical particles and dimers composed of such particles; Figure 2). Furthermore, we theoretically consider the NPs to be spatially isolated and electromagnetically decoupled from other NPs, thereby neglecting any effects due to their possible collective interactions. For simplicity, the silver NPs are assigned a disk shape with a fixed thickness t=30 nm along with varying cross-section shapes (see Figure 4A–C for illustrations). The incident electric field is always polarized along the long axis of the disks to maximize the coupling to the longest-wavelength plasmonic resonances. Finally, the disks are situated on a semi-infinite GaAs substrate while covered by an ITO layer of thickness t_{ITO}=100 nm.

To understand the influence of the surrounding medium on the plasmonic response of the nanodisks, we begin by considering the extinction cross-section of a circular disk of radius R=65 nm in three different configurations: (i) homogeneously embedded in air, (ii) situated on a GaAs substrate with air above, and (iii) situated on a GaAs substrate with a covering ITO layer. The results of the simulations are presented in Figure 4A. It shows that the dipole resonance (see inset of Figure 4A for the electric field amplitude) of the disk is red-shifted due to the presence of the GaAs substrate by about 700 nm from the visible to the near-IR range. Because we are interpolating experimental data for the permittivities of Ag, GaAs, and ITO [55–57], our simulations are restricted to the wavelength range of 1000–1750 nm. Interestingly, adding the ITO layer does not, in this particular case, alter the resonance wavelength significantly, as the real part of the permittivity of ITO is around unity (i.e. like air) at the resonance wavelength (~1200 nm) [57]. However, we observe a decrease in the amplitude of the extinction cross-section due to the finite imaginary part of the permittivity of ITO. An additional important feature of ITO is that the real part of the permittivity changes sign at a wavelength of approximately λ_{ITO}=1400 nm [57], which is positive for shorter wavelengths. Thus, the plasmonic modes supported by the nanodisks that resonate below (above) λ_{ITO} will be red-shifted (blue-shifted) closer to λ_{ITO}, thereby giving rise to plasmonic resonances in the desired near-IR range from different nanodisk shapes.

One of the potential reasons for the experimentally observed absorbance enhancement in the presence of the NPs could be related to ohmic losses in the NP and not, as desired, to increased photocurrent in the semiconductor layer due to hot-electron transfer. Hence, it is important to also look at the two contributions to the extinction cross-section: the scattering and absorption cross-sections. In Figure 4B, we study an elliptical disk with the minor and major semiaxes a=50 nm and b=120 nm, respectively. We observe a dipole resonance at approximately 1600 nm. The resonance wavelength is longer than for the case of a circular disk in Figure 4A due to the increased size and aspect ratio of the disk. Importantly, we note that the main contribution to the extinction cross-section comes from scattering and not absorption. We can therefore argue that the experimentally observed absorbance enhancement is not due to ohmic dissipation in the NPs but more likely due to the hot-electron transfer to the GaAs substrate. These hot electrons could eventually be detected as an increase in a photocurrent.

Finally, we also studied the extinction cross-section of dimers composed of overlapping nanodisks with varying overlap g. The results for overlaps g=5, 10, and 15 nm are

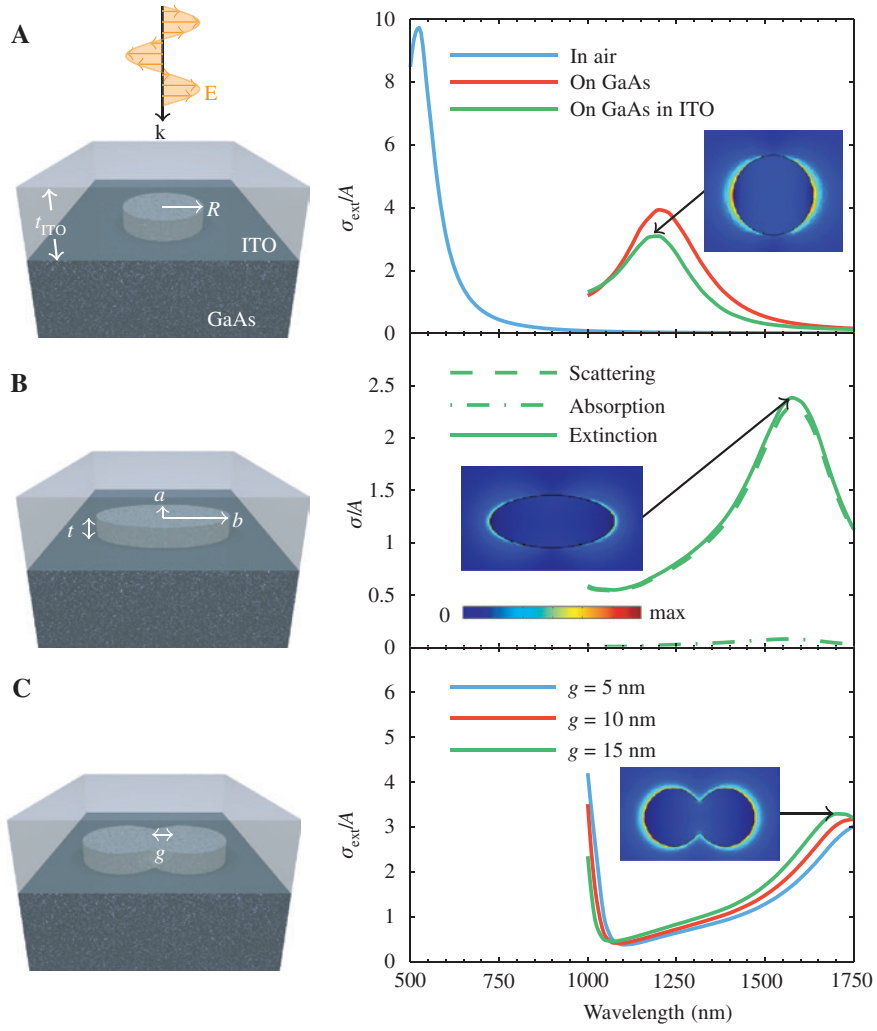

Figure 4: Resonance behavior of three characteristic shapes of silver NPs.
(A) Left: Schematic illustration of the simulation model depicting a TM plane wave impinging normal to the circular silver nanodisk of thickness t and radius R. The disk is situated on a semi-infinite GaAs substrate and covered by an ITO layer of thickness t_{ITO}=100 nm. Right: Extinction cross-section σ_{ext} normalized to the cross-section disk area A for three different cases: disk embedded in air (blue), disk on a GaAs substrate with air above (red), and disk on a GaAs substrate covered by an ITO layer. (B) Left: Similar to (A) but for an elliptical silver nanodisk with minor and major semiaxes a and b, respectively. The incident electric field is polarized along the major semiaxis. Right: Normalized scattering (dash), absorption (dash-dot), and extinction (solid) cross-sections of an elliptical disk with semiaxes a=50 nm and b=120 nm situated on a GaAs substrate with a covering ITO layer. (C) Normalized extinction cross-section of overlapping disk dimers with radius R=65 nm and varying overlap g. The sharp contact points at the overlap are rounded with a radius of 5 nm. The insets show the resonant electric field amplitude evaluated at the top interface of the disks. The dielectric functions for Ag, GaAs, and ITO are taken from experimental data [55–57].

presented in Figure 4C, which shows that the overlapping dimers produce plasmonic resonances at even longer wavelengths than elongated particles, thereby explaining the absorbance enhancement at the longest wavelengths (≥1700 nm). These bigger red-shifts occur as a result of hybridization [32], when the particles start to overlap.

Summarizing, we have theoretically shown that the three most characteristic NP shapes of our sample (i.e. circular, elliptical, and overlapping dimers) all support plasmonic resonances in the near-IR spectral range. Hence, we speculate that these resonances generate hot electrons that are transferred to the GaAs substrate.

5 EELS characterization

EELS using focused electron beams can be used to probe a variety of LSP modes [58–61], including the common bright modes but also dark plasmon modes [62, 63] as well

as higher-order modes [64, 65]. This means that, using this technique, we are able to excite with an electron beam all the dipolar resonances [66] that we found to be optically active and that are, from theoretical simulations, expected to be responsible for the broadband monotonous absorbance enhancement.

We are particularly interested in exploring the plasmonic excitations of the silver NPs produced using electroless plating. The samples needed for such analysis are prepared using, as the substrate, windows of 10-nm-thick silicon nitride (Si_3N_4) membranes on a frame of very small (3×3 mm) silicon chips of 100 μm thickness. Such substrates are commercially available and are made for transmission electron microscopy (TEM)-related measurements. On top of the membranes, an additional Si_3N_4 layer is deposited by PECVD to compensate for HF etching during the subsequent electroless process; the total thickness of the silicon nitride layer turned out to be about 20 nm, which is still transparent for the TEM and EELS measurements.

The EELS measurements are performed in an FEI Titan equipped with a monochromator and probe aberration corrector, allowing for subnanometer spatial resolution and energy resolution of 0.15±0.05 eV. To acquire EELS data, the microscope is used in the scanning TEM (STEM) mode, where the images are created by raster scanning of the subnanometer focused electron beam across the sample. At each position, an EELS spectrum can also be acquired, which produces a two-dimensional spatial map of EELS data. Such data can be used to image the near-field of the plasmonic resonances [58, 65] or simply to study individual EELS spectra.

The fabrication of the TEM samples is challenging due to the aggressiveness of the HF, used during electroless plating, on the very thin silicon nitride membrane. Figure 5A shows a STEM image of one of the best obtained samples, which is characterized by a distribution of NPs very similar to the optically characterized sample (Figure 2). We observe a wide distribution of particle sizes and shapes: particles with circular cross-sections with diameters ranging from about 20 to 70 nm along with elongated particles with different aspect ratios (even bigger than 2) and reaching major axis lengths of about 130 nm. Elongated particles approaching a wire geometry may support a series of standing-wave plasmonic resonances [67]. It is important to highlight the position distribution, which is completely random but in particular gives rise to dimers or groups of particles very close to each other (if not overlapping), with even nanometer-sized gaps. In principle, nonlocal effects may enhance the absorption too [68–70].

EELS measurements were performed on different areas of the TEM sample. In Figure 5A, the white dashed box indicates one of the areas from which an EELS map was acquired. Because our primary interest is in LSP excitations, we focus only on a few EELS spectra acquired from positions near the surface of the silver NPs, where the surface plasmon signal is the largest [65]. In particular, we consider the same characteristic shapes as in the simulations [i.e. circular (green and blue spectra in Figure 5B), elongated (red spectrum in Figure 5B), and dimers (yellow spectrum in Figure 5B)]. As in the simulations, we find that the circular-like particles exhibit, on average, larger resonance energies than the elongated particles that in turn show larger resonance energies than the dimer configuration. However, all of the plasmonic resonance energies are significantly larger than in the simulations due to the different surrounding medium. In the EELS measurements,

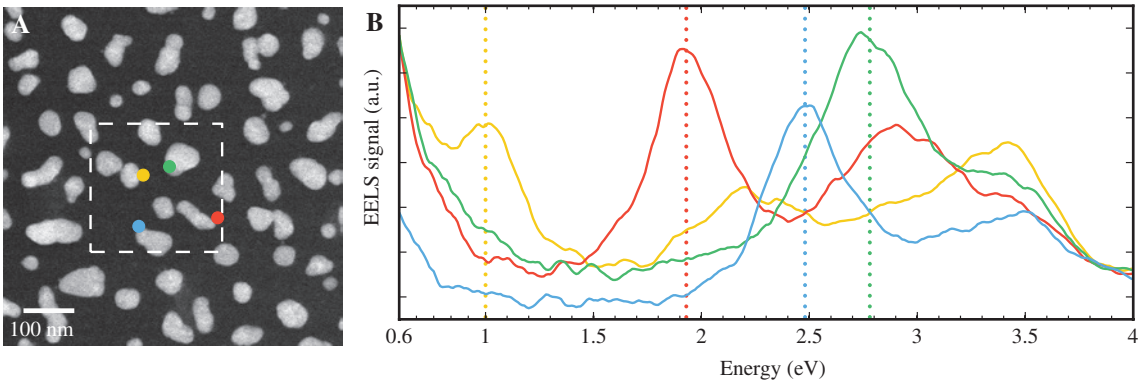

Figure 5: (A) STEM image of silver NPs deposited by electroless plating on a TEM-suitable 20-nm-thick silicon nitride membrane, showing some of the characteristic particle shapes and sizes. EELS has been collected in the area enclosed by the white dashed box. (B) EELS spectra from specific positions indicated by the colored dots. The vertical dotted lines highlight the lowest-energy resonance for each of the different particles.

the resonances are only weakly red-shifted due to the thin silicon nitride membrane compared to the GaAs-ITO environment of the samples used for optical characterization. Therefore, assigning approximately the same 700 nm redshift to the resonant wavelengths as was imposed by the substrate (as illustrated in Figure 4A), we can state that the EELS characterization fully confirmed the results of modeling.

6 Conclusions

The cheap and effective mass-production method for the deposition of silver NPs on top of semiconductor wafers has been suggested. As a result of electroless plating, random arrays of NPs of different shapes and forms are created. The optical characterization of such systems with an integration sphere reveals different spectral influence of the particle arrays on the transmission and reflection of light by the coated wafer. In the IR range beyond the GaAs bandgap (≈900 nm), the reflectance is monotonously increasing with the wavelength by 5%–10% and the transmittance drops down by 20% between 900 and 2000 nm. As a consequence of such changes, the absorbance of the system in the same range is increased by 10%–20% gradually descending to the long-wavelength edge. Meanwhile, there are no significant changes in the reflectance and transmittance of light above the "bandgap" range with wavelengths in the visible range and up to 900 nm. With numerical modeling, we have proven that the random shapes and sizes of particles deposited with the electroless method are responsible for such flat broadband absorption enhancement. Three basic shapes have been chosen for numerical modeling: circular nanodisks, elongated nanodisks, and dimers from overlapped nanodisks. The plasmonic resonance frequencies of the particles are profoundly modified by the presence of the high-index substrate: they are shifted by up to 700 nm to the longer wavelengths. The modeling results have been further validated by EELS experiments, which demonstrate the presence of the variety of resonances of the designated NPs in the specified ranges of wavelengths in the visible domain. Due to the technical requirements of EELS characterization, the NPs are deposited by the electroless plating on an extremely thin substrate of approximately 20 nm thickness. Therefore, being red-shifted by 600–700 nm with the presence of the high-index environment, such resonances would be randomly distributed in the IR range, giving a flat rise in absorption. The aforementioned properties of the random arrays of the NPs together with the exclusively cheap and fast production technology can be further exploited for various applications in photodetection, photovoltaics, and photoexcitation.

Acknowledgments: Fruitful discussions with Vladimir Shalaev and Shanhui Fan are acknowledged.

Funding: We gratefully acknowledge the support from the Danish Council for Independent Research (FNU 1323-00087). The Center for Nanostructured Graphene is sponsored by the Danish National Research Foundation project DNRF103. The A.P. Møller and Chastine Mc-Kinney Møller Foundation is gratefully acknowledged for the contribution towards the establishment of the Center for Electron Nanoscopy. S.R. acknowledges financial support from SDU project 2020.

References

[1] Baev A, Prasad PN, Ågren H, Samoć M, Wegener M. Metaphotonics: an emerging field with opportunities and challenges. Phys Rep 2015;594:1–60.
[2] Focusing in on applications. Nat Nanotechnology (Editorial) 2015;10:1. http://www.nature.com/nnano/journal/v10/n1/full/nnano.2014.332.html.
[3] Moskovits M. Surface-enhanced spectroscopy. Rev Mod Phys 1985;57:783–826.
[4] Kneipp K, Wang Y, Kneipp H, Perelman LT, Itzkan I, Dasari R, Feld MS. Single molecule detection using surface-enhanced Raman scattering (SERS). Phys Rev Lett 1997;78:1667–70.
[5] Nie S, Emery SR. Probing single molecules and single nanoparticles by surface-enhanced Raman scattering. Science 1997;275:1102–6.
[6] Taton TA, Mirkin CA, Letsinger RL. Scanometric DNA array detection with nanoparticle probes. Science 2000;289:1757–60.
[7] Schultz S, Smith DR, Mock JJ, Schultz DA. Single-target molecule detection with nonbleaching multicolor optical immunolabels. Proc Natl Acad Sci USA 2000;97:996–1001.
[8] Li KR, Stockman MI, Bergman DJ. Self-similar chain of metal nanospheres as an efficient nanolens. Phys Rev Lett 2003;91:227402.
[9] Gramotnev DR, Bozhevolnyi SI. Plasmonics beyond the diffraction limit. Nat Photon 2010;4:83–91.
[10] Kalkbrenner T, Ramstein M, Mlynek J, Sandoghdar V. A single gold particle as a probe for apertureless scanning near-field optical microscopy. J Microsc 2001;202:72–6.
[11] Zhang X, Liu Z. Superlenses to overcome the diffraction limit. Nat Mater 2008;7:435–41.
[12] Ditlbacher H, Krenn JR, Schider G, Leitner A, Aussenegg FR. Two-dimensional optics with surface plasmon polaritons. Appl Phys Lett 2002;81:1762–4.
[13] Gramotnev DK, Bozhevolnyi SI. Nanofocusing of electromagnetic radiation. Nat Photon 2014;8:14–23.

[14] Kumar K, Duan H, Hegde RS, Koh SCW, Wei JN, Yang JKW. Printing colour at the optical diffraction limit. Nat Nanotechnol 2012;7:557–61.
[15] Zhu X, Vannahme C, Højlund-Nielsen E, Mortensen NA, Kristensen A. Plasmonic colour laser printing. Nat Nanotechnol 2016;11:325–9.
[16] Engheta N. Circuits with light at nanoscales: optical nanocircuits inspired by metamaterials. Science 2007;317:1698–702.
[17] Shalaev VM. Optical negative-index metamaterials. Nat Photon 2007;1:41–8.
[18] Atwater HA, Polman A. Plasmonics for improved photovoltaic devices. Nat Mater 2010;9:205–13.
[19] Catchpole KR, Polman A. Plasmonic solar cells. Opt Express 2008;16:21793–800.
[20] Rockstuhl C, Lederer F. Photon management by metallic nanodiscs in thin film solar cells. Appl Phys Lett 2009;94:213102.
[21] Zhukovsky SV, Babicheva VE, Evlyukhin AB, Protsenko IE, Lavrinenko AV, Uskov AV. Giant photogalvanic effect in noncentrosymmetric plasmonic nanoparticles. Phys Rev X 2014;4:031038.
[22] Harutyunyan H, Martinson ABF, Rosenmann D, Khorashad LK, Besteiro LV, Govorov AO, Wiederrecht GP. Anomalous ultrafast dynamics of hot plasmonic electrons in nanostructures with hot spots. Nat Nanotechnol 2015;10:770–4.
[23] Brongersma ML, Halas NJ, Nordlander P. Plasmon-induced hot carrier science and technology. Nat Nanotechnol 2015;10:25–34.
[24] García de Abajo FJ. Colloquium: Light scattering by particle and hole arrays. Rev Mod Phys 2007;79:1267–90.
[25] Ebbesen TW, Lezec HJ, Ghaemi HF, Thio T, Wolff PA. Extraordinary optical transmission through sub-wavelength hole arrays. Nature 1998;391:667–9.
[26] Braun J, Gompf B, Kobiela G, Dressel M. How holes can obscure the view: suppressed transmission through an ultrathin metal film by a subwavelength hole array. Phys Rev Lett 2009;103:203901.
[27] Xiao S, Mortensen NA. Surface-plasmon-polariton-induced suppressed transmission through ultrathin metal disk arrays. Opt Lett 2011;36:37–9.
[28] Pillai S, Green MA. Plasmonics for photovoltaic applications. Sol Energy Mater Sol Cells 2010;94:1481–6.
[29] Rechberger W, Hohenau A, Leitner A, Krenn JR, Lamprecht B, Aussenegg FR. Optical properties of two interacting gold nanoparticles. Opt Commun 2003;220:137–41.
[30] Auguié B, Barnes WL. Collective resonances in gold nanoparticle arrays. Phys Rev Lett 2008;101:143902.
[31] Prodan E, Radloff C, Halas NJ, Nordlander P. A hybridization model for the plasmon response of complex nanostructures. Science 2003;302:419–22.
[32] Raza S, Wubs M, Bozhevolnyi SI, Mortensen NA. Nonlocal study of ultimate plasmon hybridization. Opt Lett 2015;40:839–42.
[33] Zhukovsky SV, Babicheva VE, Uskov AV, Protsenko IE, Lavrinenko AV. Enhanced electron photoemission by collective lattice resonances in plasmonic nanoparticle-array photodetectors and solar cells. Plasmonics 2014;9:283–9.
[34] Knight MW, Sobhani H, Nordlander P, Halas NJ. Photodetection with active optical antennas. Science 2011;332:702–4.
[35] Novitsky A, Uskov AV, Gritti C, Protsenko IE, Kardynal BE, Lavrinenko AV. Photon absorption and photocurrent in solar cells below semiconductor bandgap due to electron photoemission from plasmonic nanoantennas. Prog Photovoltaics 2014;22:422–6.
[36] Moulin EA, Paetzold UW, Pieters BE, Reetz W, Carius R. Plasmon induced photoexcitation of “hot” electrons and “hot” holes in amorphous silicon photosensitive devices containing silver nanoparticles. J Appl Phys 2013;113:144501.
[37] Goykhman I, Desiatov B, Khurgin J, Shappir J, Levy U. Locally oxidized silicon surface-plasmon Schottky detector for telecom regime. Nano Lett 2011;11:2219–24.
[38] Westphalen M, Kreibig U, Rostalski J, Lüth H, Meissner D. Metal cluster enhanced organic solar cells. Sol Energy Mater Sol Cells 2000;61:97–105.
[39] Wen C, Ishikawa K, Kishima M, Yamada K. Effects of silver particles on the photovoltaic properties of dye-sensitized TiO_2 thin films. Sol Energy Mater Sol Cells 2000;61:339–51.
[40] Furube A, Du L, Hara K, Katoh R, Tachiya M. Ultrafast plasmon-induced electron transfer from gold nanodots into TiO_2 nanoparticles. J Am Chem Soc 2007;129:14852–3.
[41] Nishijima Y, Ueno K, Yokota Y, Murakoshi K, Misawa H. Plasmon-assisted photocurrent generation from visible to near-infrared wavelength using a aunanorods/TiO_2 electrode. J Phys Chem Lett 2010;1:2031–6.
[42] Kirkengen M, Bergli J, Galperin YM. Direct generation of charge carriers in c-Si solar cells due to embedded nanoparticles. J Appl Phys 2007;102:093713.
[43] Moulin E, Luo P, Pieters B, Sukmanowski J, Kirchhoff J, Reetz W, Mueller T, Carius R, Royer F-X, Stiebig H. Photoresponse enhancement in the near infrared wavelength range of ultrathin amorphous silicon photosensitive devices by integration of silver nanoparticles. Appl Phys Lett 2009;95:033505.
[44] Luo PQ, Moulin E, Sukmanowski J, Royer FX, Dou XM, Stiebig H. Enhanced infrared response of ultra thin amorphous silicon photosensitive devices with Ag nanoparticles. Thin Solid Films 2009;517:6256–9.
[45] Fukuda M, Aihara T, Yamaguchi K, Ling YY, Miyaji K, Tohyama M. Light detection enhanced by surface plasmon resonance in metal film. Appl Phys Lett 2010;96:153107.
[46] Desiatov B, Goykhman I, Mazurski N, Shappir J, Khurgin JB, Levy U. Plasmonic enhanced silicon pyramids for internal photoemission Schottky detectors in the near-infrared regime. Optica 2015;2:335–8.
[47] Okinaka Y, Hoshino M. Some recent topics in gold plating for electronics applications. Gold Bull 1998;31:3–13.
[48] Mallory GO, Hajdu JB, editors. Electroless plating: fundamentals & applications. Technology & engineering. Cambridge, Cambridge University Press, 1990.
[49] Ling GP, He JH, Huang L. Size control of silver nanoparticles deposited on silica dielectric spheres by electroless plating technique. J Mater Sci 2004;39:2955–7.
[50] Porter LA, Choi HC, Ribbe AE, Buriak JM. Controlled electroless deposition of noble metal nanoparticle films on germanium surfaces. Nano Lett 2002;2:1067–71.
[51] Durhuus D, Larsen MV, Andryieuski A, Malureanu R, Pizzoccherob F, Bøggild P, Lavrinenko AV. Selective electroless silver deposition on graphene edges. J Electrochem Soc 2015;162:D213–7.
[52] Malureanu R, Zalkovskij M, Andryieuski A, Lavrinenko AV. Controlled Ag electroless deposition in bulk structures with complex three-dimensional profiles. J Electrochem Soc 2010;157:K284–8.

[53] Yu ET. Nanoplasmonics for photovoltaic applications. In: Tsakalakos L, ed. Nanotechnology for photovoltaics. Chapter 10. New York, CRC Press, 2010, 391–421.
[54] Kampen T, Schuller A, Zahn DRT, Biel B, Ortega J, Perez R, Flores F. Schottky contacts on passivated GaAs(100) surfaces: barrier height and reactivity. Appl Surf Sci 2004;234:341–8.
[55] Johnson PB, Christy RW. Optical constants of the noble metals. Phys Rev B 1972;6:4370–9.
[56] Skauli T, Kuo PS, Vodopyanov KL, Pinguet TJ, Levi O, Eyres LA, Harris JS, Fejer MM, Gerard B, Becouarn K, Lallier E. Improved dispersion relations for GaAs and applications to nonlinear optics. J Appl Phys 2003;94:6447–55.
[57] Naik GV, Kim J, Boltasseva A. Oxides and nitrides as alternative plasmonic materials in the optical range. Opt Mater Express 2011;1:1090–9.
[58] Nelayah J, Kociak M, Stephan O, García de Abajo FJ, Tence M, Henrard L, Taverna D, Pastoriza-Santos I, Liz-Marzan LM, Colliex C. Mapping surface plasmons on a single metallic nanoparticle. Nat Phys 2007;3:348–53.
[59] Chu M-W, Myroshnychenko V, Chen CH, Deng J-P, Mou C-Y, García de Abajo FJ. Probing bright and dark surface-plasmon modes in individual and coupled noble metal nanoparticles using an electron beam. Nano Lett 2009;9:399–404.
[60] García de Abajo FJ. Optical excitations in electron microscopy. Rev Mod Phys 2010;82:209–75.
[61] Colliex C, Kociak M, Stéphan O. Electron energy loss spectroscopy imaging of surface plasmons at the nanometer scale. Ultramicroscopy 2016;162:A1–24.
[62] Raza S, Stenger N, Pors A, Holmgaard T, Kadkhodazadeh S, Wagner JB, Pedersen K, Wubs M, Bozhevolnyi SI, Mortensen NA. Extremely confined gap surface-plasmon modes excited by electrons. Nat Commun 2014;5:4125.
[63] Scholl JA, Garcia-Etxarri A, Aguirregabiria G, Esteban R, Narayan TC, Koh AL, Aizpurua J, Dionne JA. Evolution of plasmonic metamolecule modes in the quantum tunneling regime. ACS Nano 2016;10:1346–54.
[64] Koh AL, Bao K, Khan I, Smith WE, Kothleitner G, Nordlander P, Maier SA, McComb DW. Electron energy-loss spectroscopy (EELS) of surface plasmons in single silver nanoparticles and dimers: influence of beam damage and mapping of dark modes. ACS Nano 2009;3:3015–22.
[65] Raza S, Kadkhodazadeh S, Christensen T, Di Vece M, Wubs M, Mortensen NA, Stenger N. Multipole plasmons and their disappearance in few-nanometer silver nanoparticles. Nat Commun 2015;6:8788.
[66] Christensen T, Yan W, Raza S, Jauho A-P, Mortensen NA, Wubs M. Nonlocal response of metallic nanospheres probed by light, electrons, and atoms. ACS Nano 2014;8:1745–58.
[67] Nicoletti O, Wubs M, Mortensen NA, Sigle W, van Aken PA, Midgley PA. Surface plasmon modes of a single silver nanorod: an electron energy loss study. Opt Express 2011;19:15371–9.
[68] Mortensen NA, Raza S, Wubs M, Søndergaard T, Bozhevolnyi SI. A generalized non-local optical response theory for plasmonic nanostructures. Nat Commun 2014;5:3809.
[69] Uskov AV, Protsenko IE, Mortensen NA, O'Reilly EP. Broadening of plasmonic resonance due to electron collisions with nanoparticle boundary: a quantum mechanical consideration. Plasmonics 2014;9:185–92.
[70] Khurgin JB. How to deal with the loss in plasmonics and metamaterials. Nat Nanotechnol 2015;10:2–6.